Jaffrey-Hamel flow features of Oldroyd-B model through intersecting plates

Sohail Rehman [a,*], Souhail Bouzgarrou [b,*], Hashim [c], Mehdi Akermi [d]

[a] *Department of Mathematics Islamia College, Peshawar, 25000, Pakistan*
[b] *Department of Civil Engineering, College of Engineering, Jazan University, Jazan, P.O. Box. 706, Jazan 45142, Saudi Arabia*
[c] *Department of Mathematics and Statistics, University of Haripur, 22620, Haripur, Pakistan*
[d] *Physics Department, Faculty of Sciences, Jazan University, Jazan, Saudi Arabia*

ARTICLE INFO

ABSTRACT

We evaluate the steady Jaffrey-Hamel flow of a viscoelastic fluid using Oldroyd-B model in a deformable channel formed by two intersecting plates. To be more precise, we offer a mathematical structure for computing the leading-order impacts of the fluid viscoelasticity on the flow in the setting of relaxation and temporal retardation interactions between the fixed walls of the channel. The typical dimensionless variables influencing the inter-action of fluid and structure in both wider (divergent) and narrower (convergent) channels are primarily identified. The flow originates from a source located at the apex, travel from convergent to divergent zone, and exist at the outlet to the reservoir. Only radial component of velocity contributes to the fluid velocity while the azimuthal component is zero. The fluid attributes are independent of hydraulic pressure and temperature. We highlight the respective contributions of various components of momentum equation coupled with pressure gradient along the radial and tangential direction. The pressure gradient is omitted, since gradients of visco-elastic shear stresses predominantly cause the contribution for narrower/expanding geometries. We further demonstrate that, although the pressure is minimal along the midline line for narrow geometries, viscoelas-tic stresses are equal to or greater than shear stresses across the domain. Applying the principle of momentum and mass conservations in a cylindrical polar framework, the system of governing equations are constructed. The computer based MATLAB code (bvp4c tool) is used to numerically solve the consequent set of modelled equations. The results pertaining to a Navier-Stokes fluid, and a Maxwell fluid exist as limiting instances of our formulations. Effect of inertial forces ($20 \leq Re \leq 140$) and channel opening have similar effects on converging and diverging section of the channel. A higher strain delaying time and a shorter stress relaxation phase produce an improved velocity profile, but both viscoelastic times have the opposite effect.

1. Introduction

In many real-life scenarios, the flow over a diverging or deviating channel is significant. The polymeric industry, rheological fluids in conduits and cavities, blood flow via veins and arteries, ecological and civil engineering, and aircraft are examples of this sort of flow. The flow of the viscous liquid along aligned surfaces has been extended within the framework of several unique Newtonian and non-Newtonian liquid model, in the perspective of a wide range of scientific and technical applications. For example, it will make a substantial contribution to the transmission of crucial production processes extruded die designs. Additionally, they are important for a number of scientific projects in the disciplines of engineering, biology, manufacturing, and biomechanics

(Coussot, 2014), (Boujelbene et al., 2023). This type of flow was first identified by (Jeffery, 1915) and afterward (G, 1917). An analytical elucidation to the Navier-Stokes equations was investigated by (Sadeghy et al., 2007). The Jeffery-Hamel (J-F) flow of a non-Newtonian liquids does not adhere an exact solution. However, the use of similarity vari-ables making it possible to test the viability of rheological models (constitutive relations connecting the stress vector to the rate of de-formations tensor). In response to the broad spectrum of applications in industry, numerous scientists have investigated the transmission across intersecting plate's channels in the setting of different non-Newtonian fluids. In a convergent or diverging channel with permeable walls, (Kazakia and Rivlin, 1997) reported a computational simulation for a non-Newtonian fluid following a power-law constitutive model. Later,
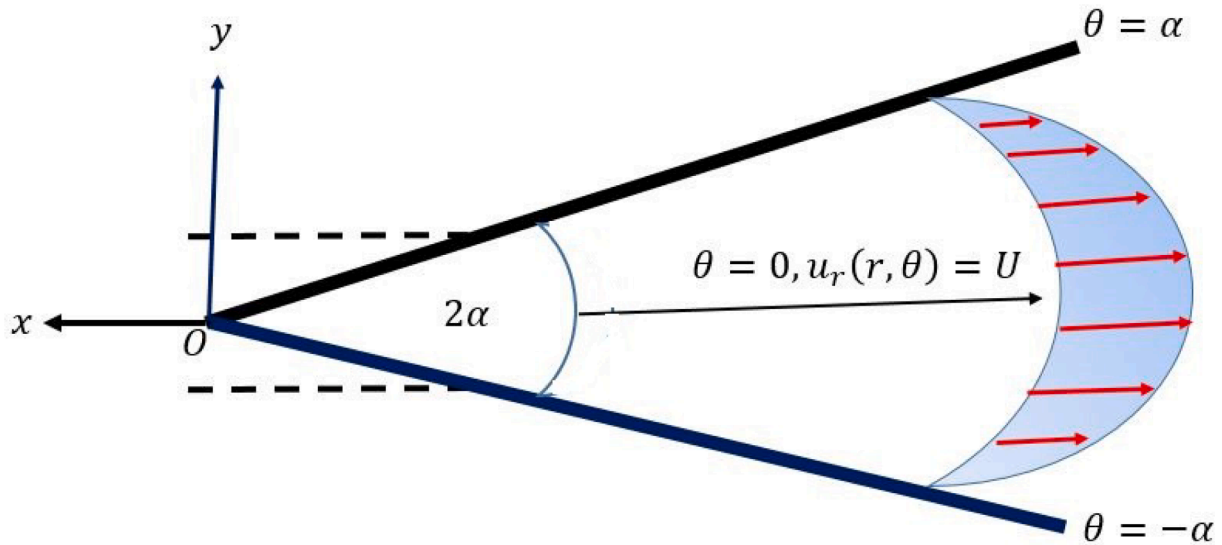
Fig. 1. Geometrical description and flow orientation.

(Strauß, 1974) explored the fundamental problem and offered the powers series approaches for the steady 2D isothermal flow of a Maxwell liquid across two colliding surfaces. (Ara et al., 2019) examined heat transmission in the J-F flow of a Bingham liquid in the backdrop of a Lorentz forces using the straightforward Bingham fluid (ignoring regularization). He assumes an optimal viscous dissipation flow while the - fluid was supplied throughout the channel. Even the preceding assumption may not be true for flows where the degree of distortion is zero at a few points in the outcome domain. Several investigator (Peddieson Jr., 1973), (Hooper et al., 1982), (Shibanuma and Kato, 1980), (Balmer, 1971), (Langlois, 1996), and (Rehman et al., 2023) examined the convergent divergent conduits flow problem in depth using different rheological models.

In response to its significance in many fields of engineering, science, and technology, especially in the material manufacturing, biological, and nuclear sectors, geophysics the dynamics of non-Newtonian fluids is currently gaining tremendous significance. Due to its applications in many fields of science, engineering, and technology, particularly in the material processing, chemical and nuclear industries, geophysics, and bioengineering, the flow of non-Newtonian fluids has recently attained enormous importance. Non-Newtonian fluids are categorized based upon the manner they behave in applied shear for an assortment of characteristics. A fluid is considered classical if the shear stress and shear rate have a direct relationship that results in an equilibrium viscosity. Since several fluids exhibit uniform viscosity but are undoubtedly not Newtonian, such as the second-order fluid, a Maxwell model, and the Oldroyd models A and B. The traditional Newtonian and the Maxwell fluid model are two specific examples of the Oldroyd-B fluid, which has recently gained a particular standing within various fluids of the rate kind. Other mathematical frameworks that can forecast the motion of such materials have been developed because of the Navier-Stokes theory limitations in representing rheologically complicated fluids used in manufacturing procedures, such as polymeric solutions, melting, and pigments. The Oldroyd-B fluid model constitutes among them (Oldroyd, 1950), (OLDROYD, 1951). This fluid, which accounts for the elastic and memory characteristics discloses that most polymers and biological fluids display, are applied in a variety of settings, and simulation findings generally agree with experimental data (Bird, 1987). (Rajagopal and Bhatnagar, 1995) explored two straightforward flows as a follow-up to their analysis of an Oldroyd-B fluid. Several researcher (Hayat et al., 2001), (Fetecau et al., 2007), (T Hayat et al., 2004), (T. Hayat et al., 2004), (Cui et al., 2022), (Cui et al., 2021), (Jan et al., 2022) explore the effect of non-Newtonian and Oldroyd-B fluid in a different geometry.

A review of the prior discussions, it appears that no work has been done on the Jeffery-Hamel flow of the Oldryod-B fluid although substantial work has been done on the conduit flow of coupled stresses fluids. As a result, the goal of the current study is to examine the flow behavior in the J-H flow of a coupled stresses fluid while handling the convergent and divergent flow zones. The two rigid boundaries, which intersect together with some angle, are chosen as flow domain. The flow is caused by a source located at the inlet and maintained under a constant pressure gradient between two boundaries of the channel. The expression of pressure gradient is negligible because we believe that the flow attributes in both sections are different and the contribution of pressure to flow characteristics are negligible as compared to fluid geometry, rheological behavior, and inertial forces. For convenience of brevity, it is believed that fluctuations in pressure and temperature have no effect on the fluid characteristics. As a result, the momentum equation, which is a partial differential equation, can be independently converted into ODE's using similarity transformation while omitting the pressure term. Numerical solutions are found for extremely nonlinear momentum equation using bvp4c routine. The flow dissemination across the conduit is determined by solving the momentum equation after finding the velocity profile and considering the flow to be a balanced viscous dissipative flow, (fluids blended thermal fluctuations through the conduit are small).

2. Conservation equations

The fundamental equations governing the flow of steady and incompressible viscoelastic fluid are presented here (Brandi et al., 2019), (Varchanis et al., 2022):

$$\nabla \bullet V = 0 \tag{1}$$

$$\rho \frac{DV}{Dt} = \nabla \bullet (-pI + \mu\dot{\gamma} + \tau) \tag{2}$$

$$\tau + \lambda \frac{\delta\tau}{\delta t} = \mu_p \dot{\gamma}. \tag{3}$$

Where, $-pI$ is the indeterminate spherical stress. The convected derivative, $\frac{DV}{Dt}$, is given as: $\frac{DV}{Dt} = \frac{\partial V}{\partial t} + V \bullet \nabla V$, $\dot{\gamma} = 2D = (\nabla V + \nabla V^{tr})$, is the rate of deformation tensor, λ_1 and λ_2 are fluid relaxation time is the polymer-contributed viscosity, respectively, ρ is the fluid density, $\nabla = \left(\frac{\partial}{\partial r}, \frac{1}{r}\frac{\partial}{\partial \theta}, \frac{\partial}{\partial z}\right)$ is the Hamiltonian operator, $\overrightarrow{V}$ is the velocity vector, τ is the stress tensor of the Oldroyd-B fluid (Bhatnagar et al., 1993), (Huang
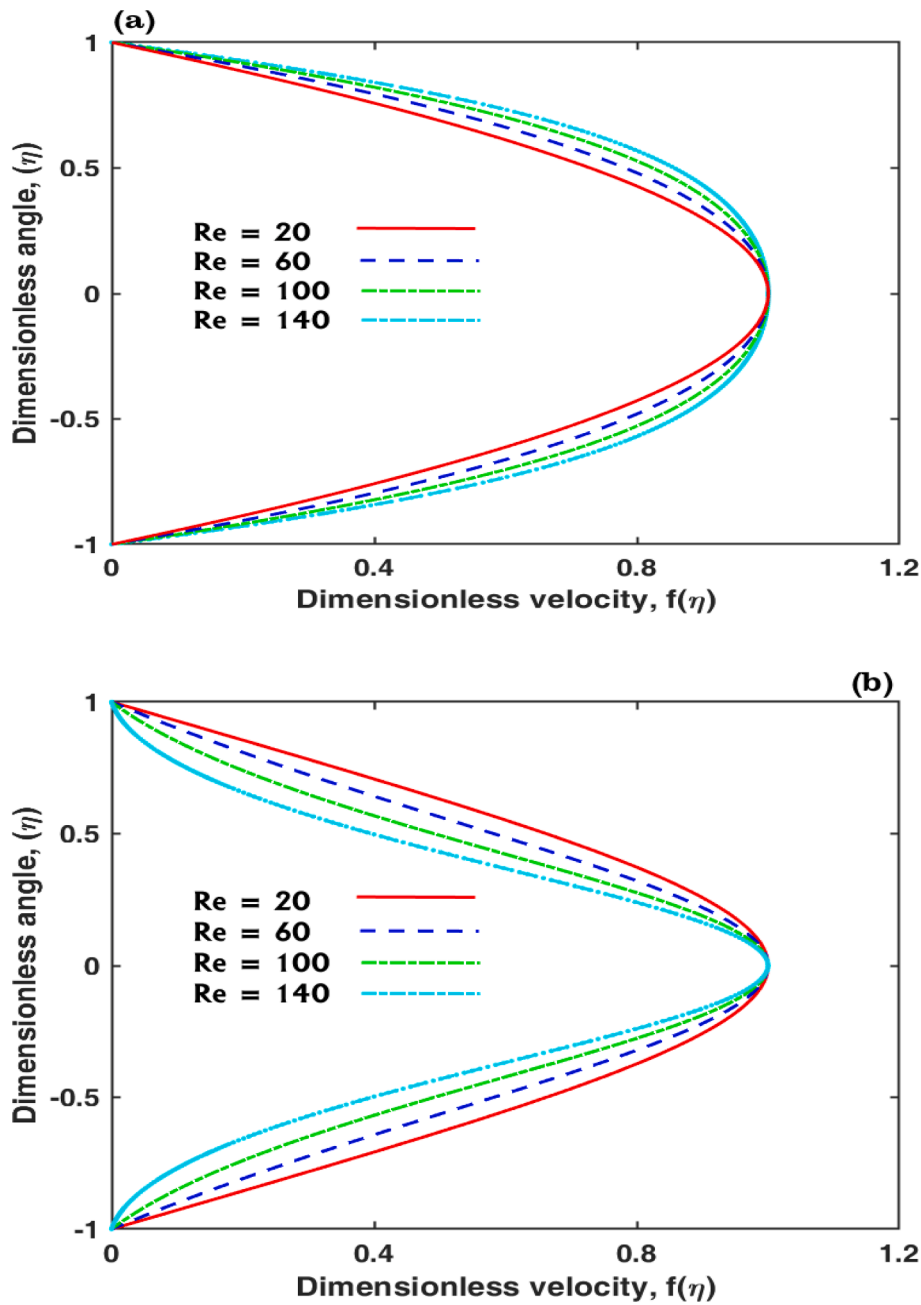
Fig. 2. Flow attributes against *Re* when $De_1 = De_2 = 0.2$, with a apex angle (a) -5^0 and (b) 5^0.

et al., 1998).

The upper convective time derivative $\frac{\delta}{\delta t}$ in equation (3) is mathematically written as (Zhao et al., 2013),

$$\frac{\delta \tau}{\delta t} = \frac{\partial \tau}{\partial t} + V \bullet \nabla \tau - \tau \bullet \nabla V - (\nabla V)^{tr} \bullet \tau \qquad (4)$$

Here, for steady flow $\frac{\partial}{\partial t} = 0$. In a limiting case $\lambda_2 = 0$, the problem revert to Maxwell's fluid (Razzaq et al., n.d.) and $\lambda_1 = 0 = \lambda_2$ the problem revert to traditional viscous fluid. Thus, the Eq. (2), simply takes the form:

$$\rho(V.\nabla)V = -\nabla p + \mu \nabla \bullet \dot{\gamma} \qquad (5)$$

3. Problem statement and formulation

The investigation of converging and diverging channels is depicted schematically in Fig. 1. It can be seen from the schematic, that the 2-dimensional conduit walls are oriented at an angle of 2α. Both the radial and z directions of the channel reach to infinite direction, having the z direction acting as the unaffected direction $\left(\frac{\partial}{\partial z} = 0\right)$ and $z = 0$. The cylindrical polar coordinate (r, θ, z) is positioned at the conduit's apex. The converging channel can be studied using the same dimensions as the diverging channel. In actuality, it is realistic to assume that the flow in a converging conduit is inadequate (Rezaee et al., 2023). By doing so, we can establish boundary constraints that apply to all sorts of networks without defining the limits for a converging channel. The flow is anticipated to be incompressible $\rho =$ constant, continuous, completely developed in terms of hydrodynamics, steady state $\left(\frac{\partial}{\partial t} = 0\right)$, and devoid of body forces. Since the flow investigation area is sufficiently removed from the channel's apex and inlet, it is believed that the velocity component in the $\theta -$ direction is zero i.e., $u_\theta(r, \theta)\hat{e}_\theta = 0$. To simplicity, we have presummated that the viscosity and density of the fluid are
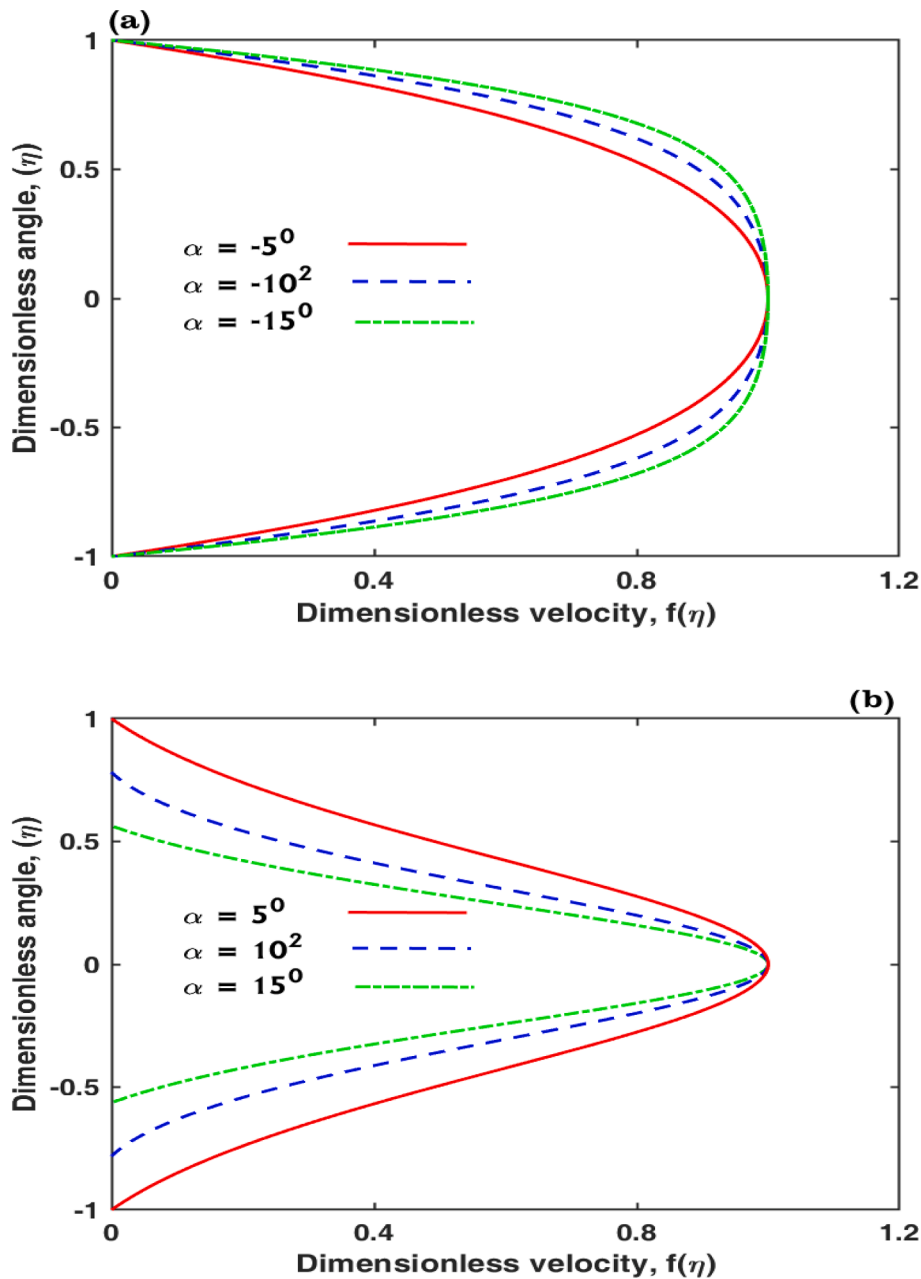
Fig. 3. Flow attributes against α when, $Re = 100, De_1 = De_2 = 0.2$, with a apex angle (a) $-5^0, -10^0, -15^0$ and (b) $5^0, 10^0, 15^0$.

unaffected by the fluid temperature and pressure. The velocity vector is interpreted as $V = u_r(r,\theta)\widehat{e}_r$.

Assuming velocity vector $V = u_r(r,\theta)\widehat{e}_r$, the tensor $\dot{\gamma}$ becomes:

$$\dot{\gamma} = \begin{pmatrix} 2\dfrac{\partial u_r(r,\theta)}{\partial r} & \dfrac{1}{r}\dfrac{\partial u_r(r,\theta)}{\partial \theta} & 0 \\ \dfrac{1}{r}\dfrac{\partial u_r(r,\theta)}{\partial \theta} & 2\dfrac{u_r(r,\theta)}{r} & 0 \\ 0 & 0 & 0 \end{pmatrix} \tag{6}$$

Taking divergence of $\dot{\gamma}$, we have

$$\nabla\dot{\gamma} = \left(\dfrac{\partial^2 u_r(r,\theta)}{\partial r^2} + \dfrac{1}{r^2}\dfrac{\partial^2 u_r(r,\theta)}{\partial \theta^2} + \dfrac{1}{r}\dfrac{\partial u_r(r,\theta)}{\partial r} - \dfrac{u_r(r,\theta)}{r^2}\right)\widehat{e}_r$$
$$+ \left(\dfrac{3}{r^2}\dfrac{\partial u_r(r,\theta)}{\partial \theta} + \dfrac{1}{r}\dfrac{\partial^2 u_r(r,\theta)}{\partial r\partial \theta}\right)\widehat{e}_\theta \tag{7}$$

The term $(V \bullet \nabla)V$ elucidate the inertial expression and written as:

$$(V \bullet \nabla)V = u_r(r,\theta)\dfrac{\partial u_r(r,\theta)}{\partial r}\widehat{e}_r. \tag{8}$$

Using Eq. (6), (7) and (8), in Eq. (5), we have

$$\rho\dfrac{\partial p}{\partial r} = -u_r(r,\theta)\dfrac{\partial u_r(r,\theta)}{\partial r} - \lambda_1\left[u_r^2(r,\theta)\dfrac{\partial^2 u_r(r,\theta)}{\partial r^2}\right] + \mu\left(\dfrac{1}{r^2}\dfrac{\partial^2 u_r(r,\theta)}{\partial \theta^2}\right)$$
$$+ \mu\lambda_2\left(\dfrac{u_r(r,\theta)}{r^2}\dfrac{\partial^3 u_r(r,\theta)}{\partial r\partial\theta^2} - \dfrac{u_r(r,\theta)}{r^3}\dfrac{\partial^2 u_r(r,\theta)}{\partial\theta^2} - \dfrac{2}{r^3}\left(\dfrac{\partial u_r(r,\theta)}{\partial\theta}\right)^2\right), \tag{9}$$

$$\rho\left(1 + \lambda_1\dfrac{\partial}{\partial t}\right)\dfrac{1}{r}\dfrac{\partial p}{\partial\theta} = 2\mu\dfrac{1}{r^2}\dfrac{\partial u_r(r,\theta)}{\partial\theta} - 6\mu\lambda_2\dfrac{u_r(r,\theta)}{r^3}\dfrac{\partial u_r(r,\theta)}{\partial\theta}. \tag{10}$$

The realistic no slip-boundary conditions at the inlet and wall are (Rezaee et al., 2023), (Hashim et al., 2022):
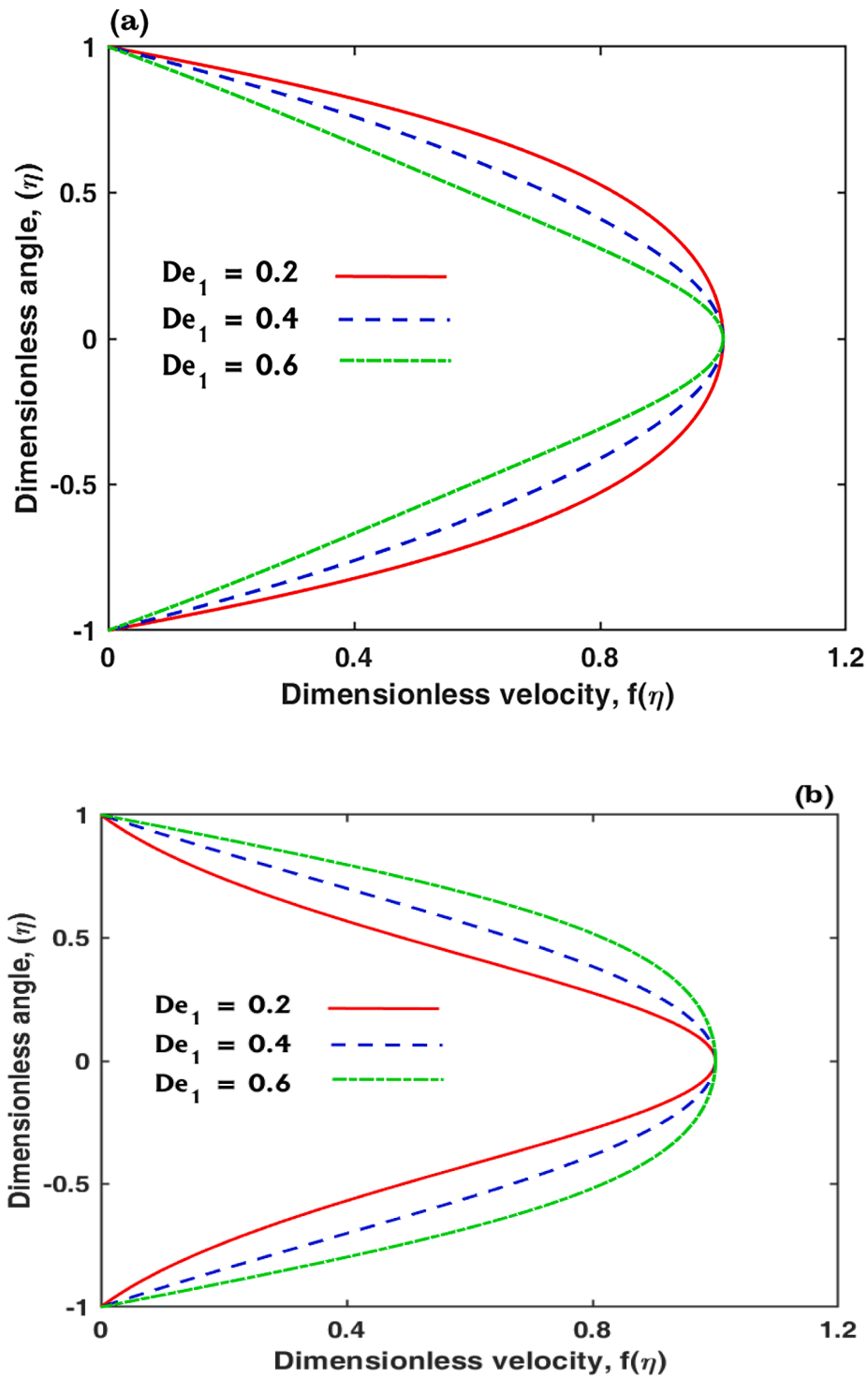
As $(\theta \to 0)$:

Fig. 4. Flow attributes against De_1 when $Re = 100, De_2 = 0.2$, with a apex angle (a) -5^0 and (b) 5^0.

$$u_r(r,\theta) = U, \frac{\partial u_r(r,\theta)}{\partial \theta} = 0, \qquad (11)$$

As $(\theta \to \pm \alpha)$:

$$u_r(r,\theta) = 0. \qquad (12)$$

The continuity equation yield to a dimensional velocity $u_r(r,\theta)r = F(\theta)$, implying $u_r(r,0) = F(0) = rU$, where U is the midline velocity.

The total volumetric flux crossing the channel can be estimated using the following relation:

$$\widehat{Q} = \int_{-\alpha}^{\alpha} r u_r(r,\theta) d\theta \qquad (13)$$

The positive and negative flux correspond to inflow and outflow at the inlet of the channel.

Adopting the dimensionless procedure, we introduce the following scaling variables (Rezaee et al., 2023), (Hashim et al., 2022):

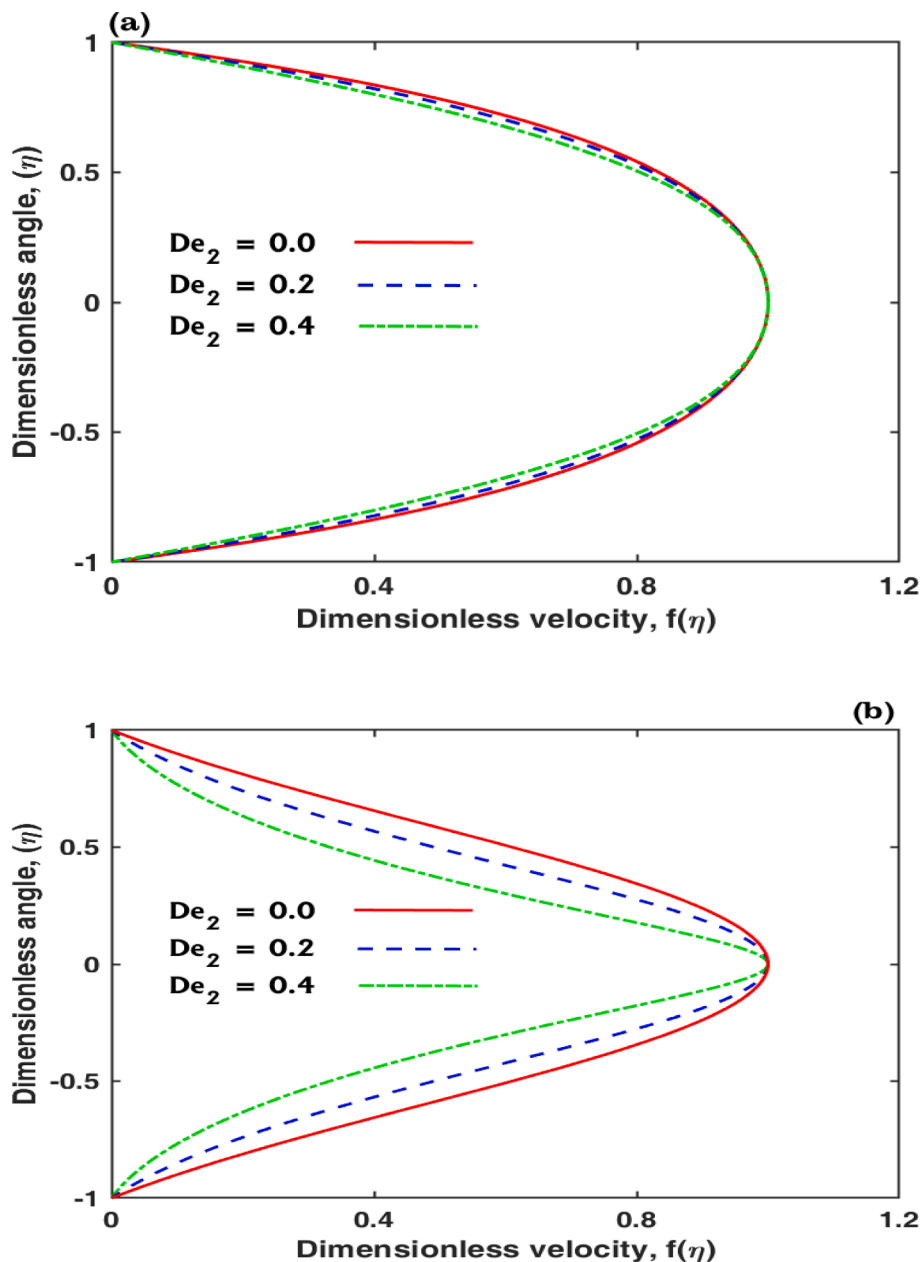$$\frac{F(\theta)}{rU} = f(\eta), \text{ where } \eta = \frac{\theta}{\alpha} \qquad (14)$$

Fig. 5. Flow attributes against De_2 when $Re = 100, De_1 = 0.2$, with a apex angle (a) -5^0 and (b) 5^0.

Table 1
Validation of the present outcomes with available studies for $f(\eta)$, when $De_1 = 0, De_2 = 0$ (vsicous fluid).

η	(Bég et al., 2022)			Present study		
	$Re = 110\, \alpha = 3^0$	$Re = 80$ $\alpha = -5^0$	$Re = 50\, \alpha = 5^0$	$Re = 110\, \alpha = 3^0$	$Re = 80\, \alpha = -5^0$	$Re = 50\, \alpha = 5^0$
0	1	1	1	1	1	1
0.1	0.97923571	0.99596063	0.98243124	0.9789	0.9955	0.9818
0.2	0.91926589	0.98327554	0.93122597	0.9188	0.9830	0.9309
0.3	0.82653362	0.96017991	0.85061063	0.8261	0.9201	0.8502
0.4	0.71022119	0.92352159	0.74679081	0.7101	0.9231	0.7469
0.5	0.58049946	0.86845888	0.62694818	0.5804	0.8882	0.6263
0.6	0.44693507	0.78809092	0.49823446	0.4461	0.7880	0.4980
0.7	0.31740843	0.67314363	0.36696635	0.3169	0.6728	0.3664
0.8	0.19764109	0.51199109	0.23812375	0.1972	0.5118	0.2379
0.9	0.09123042	0.29155874	0.11515193	0.0910	0.2913	0.1149
1	0	0	0	0	0	0

Here, $f(\eta)$ signifies the normalized veloicty. η symbolizes a dimensionelss angle, and $\widehat{Q}^*$ is the volumetric flow rate between the upper and lower plates of the conduit:

$$\widehat{Q}^* = \frac{\widehat{Q}}{Ur\alpha} = \int_{-1}^{1} f(\eta)d\eta \tag{15}$$

Implementing Eq. (14) into Eq. (9) and (10), and omitting the pressure gradient terms, the governing PDE's takes the following normalized form:

$$(f'' + 4\alpha^2 f') + 2\alpha Reff' - 6\alpha ReDe_1 f^2 f' - De_2 \left(6f'f'' + 2ff''' + 24\alpha^2 ff'\right) = 0 \tag{16}$$

with the following geometric restictions at the midline and wall

$$f = 1, \ f' = 0, \ \text{as } \eta \to 0 \text{ and } f = 0. \text{ As } \eta \to \pm 1 \tag{17}$$

Where $Re = \frac{\alpha r U}{\nu}$: Reynolds number, $De_1 = \frac{\lambda_1 U}{r}$: First Deborah numbers, $De_2 = \frac{\lambda_1 U}{r} \frac{\mu}{\mu+\mu_p} = De_2 = De_1 \frac{\mu}{\mu+\mu_p}$: Second Deborah numbers, respectively.

The problem Eq. (17) revert to classical Jaffrey-Hamel by taking $De_1 = De_2 = 0$.

4. Computational solution

A computational technique bvp4c is durable and capable for managing this kind of complex boundary value problem. The MATLAB bvp4c (Kierzenka and Shampine, 2001) process is a simple and user-friendly tool that uses finite- difference algorithm to handle this challenging task. The problem is reverted to first order using shooting mechanism. Establishing a preliminary guess at a various mesh point, the results are produced by boosting the step size $\Delta\eta = 0.01$ unless the needed precision 10^{-6} is obtained.

We delineate different variables:

$$\Xi_1 = f, \Xi_2 = f', \Xi_3 = f'', \tag{18}$$

$$\Xi\Xi1 = y_3'$$
$$= \frac{\left(-4\alpha^2\Xi_2 - 2\alpha Re\Xi_1\Xi_2 + 6\alpha ReDe_1\Xi_1^2\Xi_2 - De_2(6\Xi_2\Xi_3 + 24\alpha^2\Xi_1\Xi_2)\right)}{1 - 2De_2\Xi_1}, \tag{19}$$

$$\Xi_1(0) = 1, \Xi_2(0) = 0, \Xi_1(\pm 1) = 0 \tag{20}$$

If the outcome does not satisfy the precision requirements, the solver modifies the mesh structure and keeps going until the accuracy requirements of 10^{-6} are satisfied.

5. Results and discussions

The behavior of flow $f(\eta)$ against various physical parameters is depicted in Fig. 2 − 5. The lower and upper portion of the channel are taken within the domain of $\eta \in [0, 1]$ and $\eta \in [-1, 0]$, respectively. Similar effects of Reynold number Re and channel semi-apex angle on the velocity profile can be seen in Figs. 2 and 3. In a diverging channel, a rise in Re and α reduces the gradient of velocity at the surface and slows down the fluid constituents in some manner, which lowers the surface shear stress. The decrease in the wall shear stresses caused by Re and α indicates the development of an unfavorable pressure gradient, which result in the separation of flow phenomena in divergent conduit. It is intriguing to note that the conduit apex angle and the Reynolds number influence the flow in opposite manner in a converging channel. Physically, the overall dimension of the velocity contour and the gradient of velocity at the boundary grow with increasing Reynolds number and channel apex angle. The impact of first De_1 and second Deborah number De_2 are plotted in Figs. 4 and 5. The parameter De_1 refers to relaxation

time λ_1, which spectacles a decline in momentum resulting from the fluid viscoelastic characteristic. The temporal relaxation parameter λ_1 is accountable for Deborah number De_1, which is present in the non-dimensional momentum equation (17). Physical, since momentum is associated with increased values of the material parameter De_1 therefore stronger viscous forces repel fluid molecules. Additionally, the flow rate declines because of amplified friction caused by the contracting channel (Fig. 4(a)). As a result, velocity of fluid particles decreases as relaxation time extends the elastic forces that govern the fluid mobility. Thus, deformation rate develops, and the fluid ultimately take more time to pretend solid-like characteristics. Fig. 4b suggests that the motion of fluid constituents adjacent to the boundary speeds up more intensely as De_1 increases (for instance, by raising the quantity of the polymers additives). Due to the fluid components unilateral and bilateral extensions, significant elastic stresses develop in the flow direction. The Deborah number De_2 on the other hand, exhibits a reverse behavior, resulting in a decrease in the flow fields in both conduits, as seen in Fig. 5a and 5b. Additionally, it can be seen from Fig. 4b, a significant fall in the fluid velocity is observed for diverging flow fields with increase in De_2. The rise in elongational stresses explains that there is an interruption in the particle transfer velocity caused by its elastic properties when De_2 is elevated. It is also important to remember that the fluid elements of the flow pattern constantly return in a radial manner. Moreover, the results of the current study and existing works are validated in Table 1. One can observe an excellent agreements between current and published works.

6. Final remarks

We provide a mathematical model and computational results for the flow features of Oldroyd-B fluid within intersecting surfaces having convergent and divergent cross sections. This formulation is typically uncommon in published work. The self-similar solution is accompanied by computational solutions using the Bvp4c method. Modelling viscoelastic fluid with rising Deborah numbers allows us to understand how the viscous and elasticity affects the velocity field of viscoelastic fluid in conduits, ducts, and cavities. At the conclusion, the findings are cross-checked against data that have already been published in the available literature. From the current investigation, the following conclusions may be drawn:

- With increased Reynolds number Re (inertial force) in converging channel, a sharper profile can be achieved at the conduit midline.
- The effect of inertial forces Re and apex angle α are similar for both conduits.
- The increased channel width and inertial factor for favorable pressure gradient in converging section, while conflicting behavior was seen in divergent section.
- The higher estimation of time relaxation λ_1 detract the flow field in diverging conduit.
- With higher estimation of retardation time λ_2, the distribution of flow diminished in both sections.

The analysis can be extended by taking the slip at the interface (lubricated walls), heat and mass transfer attributes, and more realistic situation (nozzle design).

Declaration of competing interest

The authors declare that they have no known competing financial interests or personal relationships that could have appeared to influence the work reported in this paper.

Acknowledgment

research work through the project number ISP23-104.

Appendix A. Supplementary material

References

Ara, A., Khan, N., Sultan, F., Ullah, S., 2019. Numerical simulation of Jeffery-Hamel flow of bingham plastic fluid and heat transfer in the presence of magnetic field. Appl. Comput. Math. 18, 135–148.

Balmer, R.T., 1971. Similarity solutions for the converging or diverging steady flow of non-newtonian elastic power law fluids with wall suction or injection. Part I: Two-dimensional channel flow. AIChE Journal.

Bég, O.A., Bég, T., Khan, W.A., Uddin, M.J., 2022. Multiple slip effects on nanofluid dissipative flow in a converging/diverging channel: A numerical study. Heat Transf. 51, 1040–1061. https://doi.org/10.1002/htj.22341.

Bhatnagar, R.K., Rajagopal, K.R., Gupta, G., 1993. Flow of an Oldroyd-B fluid between intersecting planes. J. Nonnewton. Fluid Mech. 46, 49–67. https://doi.org/10.1016/0377-0257(93)80003-T.

Bird, R.B., 1987. Dynamics of Polymeric Liquids, Volume 1: Fluid Mechanics. Wiley.

Boujelbene, M., Rehman, S., Alqahtani, S., Alshehery, S., 2023. Second law assessment of injected nanoparticles to blood flow with thermal radiation and magnetic field in conduit artery. J. Taiwan Inst. Chem. Eng. 150, 105074 https://doi.org/10.1016/j.jtice.2023.105074.

Brandi, A.C., Mendonça, M.T., Souza, L.F., 2019. DNS and LST stability analysis of Oldroyd-B fluid in a flow between two parallel plates. J. Nonnewton. Fluid Mech. 267, 14–27. https://doi.org/10.1016/j.jnnfm.2019.03.003.

Coussot, P., 2014. Yield stress fluid flows: A review of experimental data. J. Nonnewton. Fluid Mech. 211, 31–49. https://doi.org/10.1016/j.jnnfm.2014.05.006.

Cui, J., Farooq, U., Jan, A., Elbashir, M.K., Khan, W.A., Mohammed, M., Alhussain, Z.A., Ul Rahman, J., 2021. Significance of nonsimilar numerical simulations in forced convection from stretching cylinder subjected to external magnetized flow of sisko fluid. J. Math. (Wuhan) 2021, e9540195.

Cui, J., Jan, A., Farooq, U., Hussain, M., Khan, W.A., 2022. Thermal analysis of radiative Darcy-Forchheimer nanofluid flow across an inclined stretching surface. Nanomaterials 12, 4291. https://doi.org/10.3390/nano12234291.

Fetecau, C., Prasad, S.C., Rajagopal, K.R., 2007. A note on the flow induced by a constantly accelerating plate in an Oldroyd-B fluid. App. Math. Model. 31, 647–654. https://doi.org/10.1016/j.apm.2005.11.032.

G, H., 1917. Spiralformige Bewegungen Zaher Flussigkeiten 25, 34–60.

Hashim, Rehman, S., Mohamed Tag Eldin, E., Bafakeeh, O.T., Guedri, K., 2022. Coupled energy and mass transport for non-Newtonian nanofluid flow through non-parallel vertical enclosure. Ain Shams Engineering Journal 102023. https://doi.org/10.1016/j.asej.2022.102023.

Hayat, T., Siddiqui, A.M., Asghar, S., 2001. Some simple flows of an Oldroyd-B fluid. Int. J. Eng. Sci. 39, 135–147. https://doi.org/10.1016/S0020-7225(00)00026-4.

Hayat, T., Khan, M., Ayub, M., 2004. Exact solutions of flow problems of an Oldroyd-B fluid. Appl. Math Comput. 151, 105–119. https://doi.org/10.1016/S0096-3003(03)00326-6.

Hayat, T., Nadeem, S., Asghar, S., 2004. Hydromagnetic couette flow of an Oldroyd-B fluid in a rotating system. Int. J. Eng. Sci. 42, 65–78. https://doi.org/10.1016/S0020-7225(03)00277-5.

Hooper, A., Duffy, B., Moffatt, K., 1982. Flow of fluid of non-uniform viscosity in converging and diverging channels. J. Fluid Mech. 117, 283–304. https://doi.org/10.1017/S0022112082001633.

Huang, P.Y., Hu, H.H., Joseph, D.D., 1998. Direct simulation of the sedimentation of elliptic particles in Oldroyd-B fluids. J. Fluid Mech. 362, 297–326. https://doi.org/10.1017/S0022112098008672.

Jan, A., Mushtaq, M., Farooq, U., Hussain, M., 2022. Nonsimilar analysis of magnetized Sisko nanofluid flow subjected to heat generation/absorption and viscous dissipation. J. Magn. Magn. Mater. 564, 170153 https://doi.org/10.1016/j.jmmm.2022.170153.

Jeffery, G.B., 1915. L. The two-dimensional steady motion of a viscous fluid. The London, Edinburgh, and Dublin Philosophical Magazine and Journal of Science 29, 455–465. https://doi.org/10.1080/14786440408635327.

Kazakia, J.Y., Rivlin, R.S., 1997. Flow of a viscoelastic fluid between eccentric rotating cylinders and related problems, in: Barenblatt, G.I., Joseph, D.D. (Eds.), Collected Papers of R.S. Rivlin: Volume I and II. Springer, New York, NY, pp. 2148–2158. https://doi.org/10.1007/978-1-4612-2416-7_142.

Kierzenka, J., Shampine, L.F., 2001. A BVP solver based on residual control and the Maltab PSE. ACM Trans. Math. Softw. 27, 299–316. https://doi.org/10.1145/502800.502801.

Langlois, W.E., 1996. Steady Flow of Slightly Viscoelastic Fluids, in: Carroll, M.M., Hayes, M.A. (Eds.), Nonlinear Effects in Fluids and Solids. Springer US, Boston, MA, pp. 189–225. https://doi.org/10.1007/978-1-4613-0329-9_8.

Oldroyd, J.G., 1950. On the Formulation of Rheological Equations of State. Proceedings of the Royal Society of London Series A 200, 523–541. https://doi.org/10.1098/rspa.1950.0035.

OLDROYD, J.G., 1951. THE MOTION OF AN ELASTICO-VISCOUS LIQUID CONTAINED BETWEEN COAXIAL CYLINDERS. I. The Quarterly Journal of Mechanics and Applied Mathematics 4, 271–282. https://doi.org/10.1093/qjmam/4.3.271.

Peddieson Jr., J., 1973. Wedge and cone flows of viscoelastic liquids. AIChE J. 19, 377–379. https://doi.org/10.1002/aic.690190229.

Rajagopal, K.R., Bhatnagar, R.K., 1995. Exact solutions for some simple flows of an Oldroyd-B fluid. Acta Mech. 113, 233–239. https://doi.org/10.1007/BF01212645.

Razzaq, R., Farooq, U., Mirza, H.R., n.d. Nonsimilar forced convection analysis of maxwell nanofluid flow over an exponentially stretching sheet with convective boundary conditions. ZAMM - Journal of Applied Mathematics and Mechanics / Zeitschrift für Angewandte Mathematik und Mechanik n/a, e202200623. https://doi.org/10.1002/zamm.202200623.

Rehman, S., Hashim, T., Y., Alqahtani, S., Alshehery, S., Eldin, S.M.,, 2023. A renovated Jaffrey-Hamel flow problem and new scaling statistics for heat, mass fluxes with Cattaneo-Christov heat flux model. Case Stud. Therm. Eng. 43, 102787 https://doi.org/10.1016/j.csite.2023.102787.

Rezaee, D., Samari, A., Mirsaeidi, A., 2023. Heat transfer in the Jeffery-Hamel flow of a yield-stress fluid. Int. J. Heat Mass Transf. 216, 124531 https://doi.org/10.1016/j.ijheatmasstransfer.2023.124531.

Sadeghy, K., Khabazi, N., Taghavi, S.-M., 2007. Magnetohydrodynamic (MHD) flows of viscoelastic fluids in converging/diverging channels. Int. J. Eng. Sci. 45, 923–938. https://doi.org/10.1016/j.ijengsci.2007.05.007.

Shibanuma, H., Kato, H., 1980. Diverging and Converging Flows of Dilute Polymer Solutions : 2nd Report, Universal Velocity Profile of Turbulent Diverging Flow. https://doi.org/10.1299/JSME1958.23.1148.

Strauß, K., 1974. Die Strömung einer einfachen viskoelastischen Flüssigkeit in einem konvergenten Kanal. Acta Mech. 20, 233–246. https://doi.org/10.1007/BF01175926.

Varchanis, S., Tsamopoulos, J., Shen, A.Q., Haward, S.J., 2022. Reduced and increased flow resistance in shear-dominated flows of Oldroyd-B fluids. J. Nonnewton. Fluid Mech. 300, 104698 https://doi.org/10.1016/j.jnnfm.2021.104698.

Zhao, M., Wang, S., Wei, S., 2013. Transient electro-osmotic flow of Oldroyd-B fluids in a straight pipe of circular cross section. J. Nonnewton. Fluid Mech. 201, 135–139. https://doi.org/10.1016/j.jnnfm.2013.09.002.